RSC Chemical Biology

ROYAL SOCIETY OF CHEMISTRY

PAPER

View Article Online
View Journal

Cite this: DOI: 10.1039/d6cb00073h

Prochelators modulate azole activity against *Candida albicans* in a metal-dependent manner

Madeline Ann Merriman,[a] Catherine A. Denning-Jannace,[a] Andrea Barboza Hurtado,[a] Francesca A. Vaccaro,[a] Yu-Shien Sung,[b] Elisa Tomat[bc] and Katherine J. Franz*[a]

Received 26th February 2026,
Accepted 21st April 2026

DOI: 10.1039/d6cb00073h

rsc.li/rsc-chembio

Candida albicans is an opportunistic fungal pathogen of growing clinical concern, in part due to antifungal drug tolerance. Here we report a thiol-activated prochelation strategy that modulates the activity of azole antifungals against *C. albicans* in a manner influenced by the degree of azole stress as well as the metal composition of the growth medium. We identify two disulfide-linked prochelators containing aroylhydrazone $(AH1\text{-}S)_2$ or thiosemicarbazone $(IT1\text{-}S)_2$ structures that impact *C. albicans* growth in both a standard laboratory strain and a fluconazole-resistant clinical isolate. A combination of metal analysis and EPR spectroscopy of treated cells shows that $(AH1\text{-}S)_2$ redistributes intracellular iron stores by forming an intracellular iron chelator complex. We also show that $(AH1\text{-}S)_2$ promotes copper accumulation under otherwise non-toxic copper conditions, resulting in fungicidal activity.

Introduction

Candida albicans is a commensal fungal organism that can cause life-threatening disease in immunocompromised individuals.[1,2] Current antifungal therapies rely on a limited number of drug classes with declining efficacy against emerging resistant strains, although a few new options are in development.[3–6] Among the most widely used antifungals are the azoles (Fig. 1), a class introduced in the 1980s that remains central to clinical management of fungal infections. Azoles disrupt the biosynthetic pathway of ergosterol, the fungal analogue of cholesterol, by axially coordinating the heme iron of lanosterol-14α-demethylase, a cytochrome P450 enzyme of the Cyp51 family.[7,8] This coordination prevents O_2 activation and subsequent lanosterol demethylation, leading to accumulation of toxic sterols, membrane instability, and fungistatic growth arrest.[9]

C. albicans adapts to azole stress in a number of well-documented ways, including overexpression of the gene encoding Cyp51 (*ERG11*) and the upregulation of efflux pumps to decrease intracellular drug concentration.[10–14] The fungus also alters metal homeostasis, particularly of iron and copper, in response to antifungal pressure. Although iron depletion has been shown to sensitize *C. albicans* to azoles, excess iron can promote resistance to some antifungals.[15,16] *C. albicans* exposed to fluconazole in cell culture have been shown to increase heme uptake, mobilize vacuolar iron stores, and alter gene expression associated with metal homeostasis, notably of copper, iron, and zinc.[17–20] These observations underscore the intimate connection between metal-dependent processes and antifungal susceptibility.

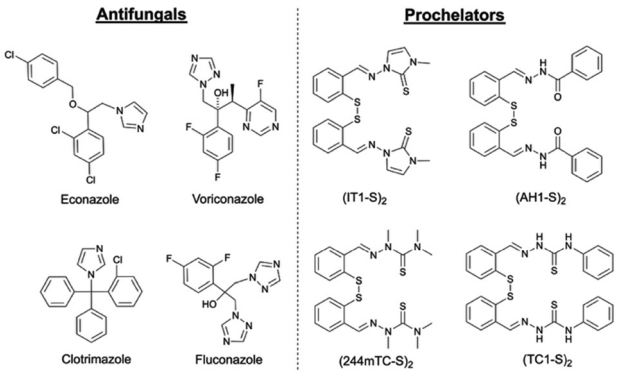

Fig. 1 Structure of antifungals and prochelators discussed in this work.

Considering *C. albicans* modulates metal homeostasis to withstand azole stress, targeting essential metal availability could be a potential therapeutic strategy to minimize drug tolerance and enhance efficacy. This concept parallels innate immune defences, wherein macrophages, monocytes, and neutrophils create iron-deplete environments to limit pathogen growth.[21] Macrophages are noted for adopting an iron-sequestering phenotype during infection.[22,23] Additionally, macrophages accumulate and compartmentalize copper to promote copper toxicity against fungal

[a] Department of Chemistry, Duke University, French Family Science Center, 124 Science Drive, Durham, North Carolina, 27708, USA. E-mail: katherine.franz@duke.edu
[b] The University of Arizona, Department of Chemistry and Biochemistry, Tucson, Arizona, 85721-0041, USA
[c] University of Vienna, Faculty of Chemistry, Institute of Inorganic Chemistry, 1090, Wien, Austria

pathogens.[24] These observations suggest that synthetic chelators and ionophores that mimic host metal regulation could serve as adjunctive antifungal agents.

The antifungal potential of metal chelators and ionophores has been explored since the 1960s, with studies reporting a mixture of both synergy and antagonism between iron chelators and conventional antifungals.[25–34] Similarly, copper ionophores and copper complexes, many of which show their own intrinsic antifungal activity, have also been shown to enhance susceptibility to fluconazole.[35–39] Conventional chelating agents, however, can act indiscriminately to bind metals from the host as well as the pathogen. A prochelation strategy that relies on activation by a particular stimulus to enable metal coordination could provide a more targeted approach. In recent years, several prochelation strategies have been designed for potential application against cancer, infectious diseases, and other conditions.[40–45]

A prochelation approach that leverages glutathione metabolism may offer a promising strategy against fungal pathogens. Evidence indicates that fungal pathogens depend on robust, functioning glutathione metabolism for virulence, as mutants with impaired glutathione metabolism show defects in hyphal formation, heightened susceptibility to macrophages and neutrophils, and attenuated virulence.[46–51] Disruption of glutathione metabolism has been shown to increase antifungal susceptibility in several yeast species.[50,52] Elevated levels of glutathione observed in fluconazole-resistant strains of *C. albicans* enable the fungus to counteract oxidative stress as part of its mechanism of drug resistance.[53] These considerations suggest that taking advantage of high glutathione levels to activate prodrugs could therefore provide a means of sensitizing pathogenic and drug-resistant fungi to antifungals.

This work set out to test the hypothesis that thiol-activated prochelators could improve azole activity against the opportunistic fungal pathogen *C. albicans.* The collection of prochelators investigated (Fig. 1) are disulfide-linked dimers that form tridentate chelators with (S,N,S) or (S,N,O) donor atoms upon activation by intracellular thiol reductants, notably glutathione.[54] They have been shown to induce cytotoxicity of ovarian and breast cancer cell lines by sequestering intracellular iron in low-spin, octahedral complexes that are inactive with respect to catalyzing formation of reactive oxygen species (ROS).[55–57] Furthermore, prochelators of this family were found to enhance the iron-sequestering phenotype of primary human macrophages.[58] Given the important role of essential metals in fungal pathogenesis and antifungal drug response, we evaluated the activity of these disulfide-linked prochelators against *C. albicans*, both alone and in combination with FDA-approved azole antifungals, as a function of iron, copper, manganese, and zinc availability in the growth medium. Using a combination of two-dimensional growth assays and spectrometric and spectroscopic techniques, this work identifies the prochelator $(AH1\text{-}S)_2$ as an agent that modulates fluconazole activity against *C. albicans* in a metal-dependent manner. Our results support a mechanism in which activation of the prochelator alters iron availability *via* intracellular formation of an iron–chelator complex, thereby sensitizing *C. albicans* to azole stress.

Results

Thiol-activated prochelators transiently suppress *C. albicans* growth

We evaluated the antifungal activity of four disulfide-based prochelators built on aroylhydrazone or thiosemicarbazone frameworks (Fig. 1), which have previously been investigated as anticancer agents.[54–56,59] Wild-type *C. albicans* strain SC5314 was grown in MOPS-buffered synthetic defined (SD) medium in the presence of increasing concentrations of each compound (Fig. 2A). Neither $(TC1\text{-}S)_2$ nor $(244mTC\text{-}S)_2$ inhibited fungal growth at concentrations up to 25 μM, a limit at which these compounds were only sparingly soluble. In contrast, both $(AH1\text{-}S)_2$ and $(IT1\text{-}S)_2$ inhibited growth in a concentration-dependent manner over 24 h (Fig. 2A). Comparable growth inhibition was observed for the fluconazole-resistant clinical isolate Y172 (Fig. 2B), indicating that the activity of these prochelators is not limited to azole-susceptible strains. By 48 h, both SC5314 and Y172 largely recovered growth to near-control levels (Fig. 2A), suggesting that the growth inhibition induced by these prochelators is transient and followed by adaptive recovery.

Given that imine C═N linkages in the prochelators tested can be hydrolytically susceptible under some conditions,[60] we assessed the stability of the active compounds to validate their speciation in the cell culture medium used for antifungal evaluation. UV–visible spectroscopy revealed that $(IT1\text{-}S)_2$ remains

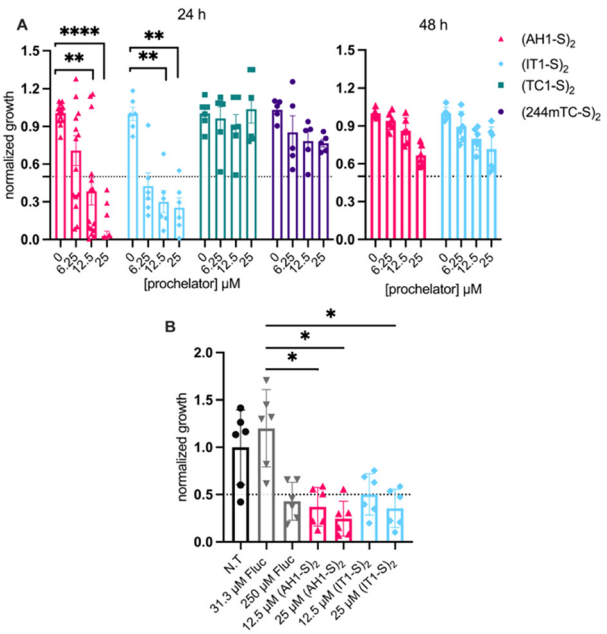

Fig. 2 (A) Effect of prochelators $(AH1\text{-}S)_2$, $(IT1\text{-}S)_2$, $(244mTC\text{-}S)_2$, and $(TC1\text{-}S)_2$ on growth of *C. albicans* strain SC5314. $(AH1\text{-}S)_2$ and $(IT1\text{-}S)_2$ decrease growth at 24 h while $(244mTC\text{-}S)_2$ and $(TC1\text{-}S)_2$ are inactive at the concentrations tested. At 48 h, cells have recovered growth. (B) $(AH1\text{-}S)_2$ and $(IT1\text{-}S)_2$ decrease growth at 24 h of *C. albicans* Y172, a fluconazole-resistant clinical isolate. Cell growth in SD medium was measured by OD_{600}. (n = 2–5 biological replicates each of n = 1–3 technical replicates). Error bars represent Standard Error of Mean (SEM). Welch ANOVA p-value < 0.0001, Dunnett's T3 multiple comparison p-value = 0.032 (*), 0.0021 (**) or < 0.0001 (****).

spectroscopically stable in SD (Fig. 3A), whereas $(AH1\text{-}S)_2$ exhibits marked time-dependent spectral changes, with a decrease in absorbance near 350 nm accompanied by a new feature emerging at 300 nm over 8 h (Fig. 3B). This behavior was not observed in MOPS buffer alone (Fig. S1), nor replicated by spectra of the putative hydrazone hydrolysis products (Fig. S2). Spectral changes induced by the reductants dithiothreitol or glutathione do not match those observed in SD but do confirm efficient thiol-triggered activation of $(AH1\text{-}S)_2$ to form the reduced chelator AH1 (Fig. S2). These results indicate that neither hydrolysis nor reduction explains the observations in SD, suggesting that components of the growth medium contribute to the instability of $(AH1\text{-}S)_2$. Systematic analysis of individual components in SD medium (Table S1) revealed a light-dependent interaction between $(AH1\text{-}S)_2$ and riboflavin as the source of the spectral changes (Fig. 3C and Fig. S3–S6). The unidentified photoproducts themselves did not inhibit growth (Fig. S7). To minimize complications due to the potential reactivity, subsequent cellular experiments with $(AH1\text{-}S)_2$ were therefore conducted under reduced-light conditions.

Together, these results indicate that disulfide-based prochelators capable of thiol activation can perturb *C. albicans* growth, but that sustained antifungal efficacy likely requires combination with additional stressors. These observations motivated subsequent studies examining the interplay of $(AH1\text{-}S)_2$ and $(IT1\text{-}S)_2$ with azole antifungals and conditions of differential metal availability.

Prochelators modulate *C. albicans* growth under azole stress

Because transient inhibition by $(AH1\text{-}S)_2$ and $(IT1\text{-}S)_2$ suggested adaptive stress responses at play, we next examined how these prochelators influence stress induced by azoles, a drug class that specifically targets an iron-dependent enzyme and disrupts metal homeostasis. Under our culture conditions, the fungistatic nature of azoles was evident at 48 h by the presence of trailing growth, defined as persistent growth in the presence of drug (Fig. 4). To assess the combinatorial effects, we performed two-dimensional broth microdilutions (checkerboards) in SD medium, varying prochelator concentrations (0–25 μM) against a range of azole concentrations selected to induce trailing growth at 48 h (fluconazole, 0–8 μM; voriconazole, 0–0.5 μM; clotrimazole, 0–0.5 μM; econazole, 0–5 μM; Fig. S8). Growth was assessed at 48 h to capture both inhibitory and adaptive responses.

Both $(AH1\text{-}S)_2$ and $(IT1\text{-}S)_2$ modulated the growth of *C. albicans* SC5314 in the presence of all four azoles tested, with outcomes dependent on the degree of azole stress (Fig. 4). At higher azole concentrations, co-treatment with either prochelator at concentrations above 6 μM completely suppressed trailing growth at 48 h, consistent with enhanced antifungal efficacy. In contrast, when paired with lower azole concentrations, the prochelators sometimes promoted growth relative to azole treatment alone, indicating that prochelator activity can

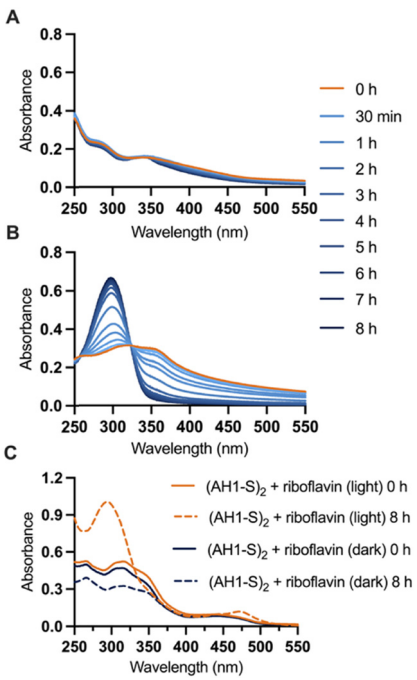

Fig. 3 UV-Vis spectra of (A) $(IT1\text{-}S)_2$ and (B) $(AH1\text{-}S)_2$ in SD medium, showing differences in their stability over time (15 μM prochelator, ambient light conditions). (C) Spectra of $(AH1\text{-}S)_2$ in MOPS buffer with riboflavin (5.3 μM) are stable over 8 h in the dark, but show a new peak at 300 nm from ambient light exposure.

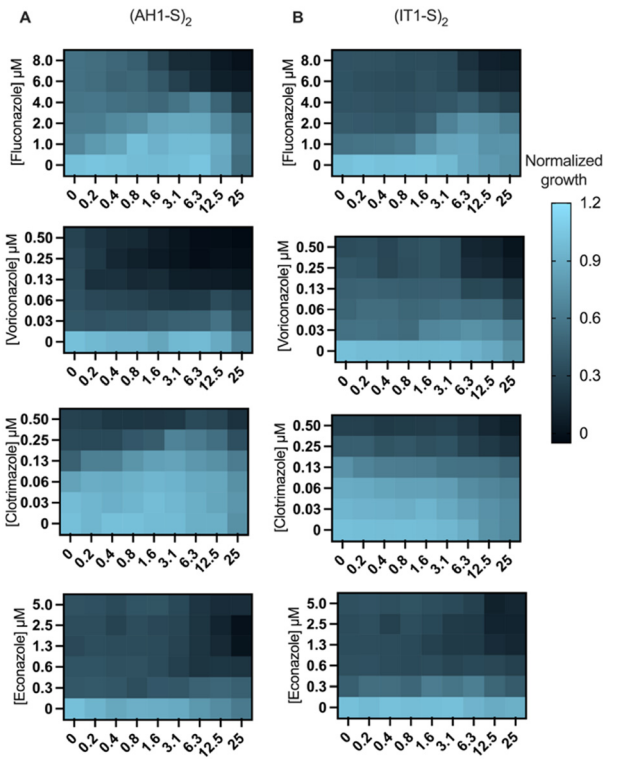

Fig. 4 Left column (A) $(AH1\text{-}S)_2$ and right column (B) $(IT1\text{-}S)_2$ modulate growth inhibitory effect of azoles against *C. albicans* SC5314 (SD medium, 48 h, n = 2–4 biological replicates of n = 1–3 technical replicates). Experiments with $(AH1\text{-}S)_2$ were performed with at least one biological replicate under minimal light exposure.

either potentiate or attenuate azole stress depending on the context. This concentration-dependent behaviour was also observed in the fluconazole-resistant clinical isolate Y172. Although higher drug concentrations were required to achieve inhibition in this strain, combined treatment with fluconazole and either prochelator fully suppressed growth at the upper concentration range (Fig. S9), demonstrating that the modulatory effects of these prochelators extend to azole-resistant strains.

To determine whether the activated chelator is responsible for the observed effects, $(AH1\text{-}S)_2$ was pre-reduced with glutathione to generate AH1 *in situ* prior to treatment. This activated chelator similarly inhibited trailing growth in the presence of fluconazole (Fig. S10). In contrast, neither the products of hydrazone hydrolysis nor the unidentified degradation product formed during the light-dependent reaction between $(AH1\text{-}S)_2$ and riboflavin inhibited trailing growth (Fig. S10). These results indicate that the thiol-activated chelator AH1 is the species responsible for modulating antifungal activity. Ambient light exposure occasionally diminished the ability of $(AH1\text{-}S)_2$ to inhibit growth in the presence of fluconazole, consistent with accelerated degradation of the active compounds under these conditions (Fig. S10). Nonetheless, growth modulation by $(AH1\text{-}S)_2$ was observed under both dark conditions and ambient light exposure (Fig. S10), indicating that the underlying biological effect is robust.

Taken together, these findings demonstrate that $(AH1\text{-}S)_2$ acts as a modulator of azole stress. The presence of the activated chelator can either sensitize *C. albicans* to azoles or confer a growth advantage, depending on the extent of azole challenge.

Metal availability shapes prochelator activity

To determine how the availability of essential d-block biometals influences the impact of the prochelators on *C. albicans* growth and susceptibility to azole stress, cells were grown in SD selectively deficient in iron, copper, manganese, or zinc, followed by metal add-back to concentrations ranging from deficient (0 μM), to sufficient (defined by metal-replete SD, Table S1), to excess (50 μM iron, zinc, or manganese, or 40 μM copper). Cells were treated with 15 μM prochelator, 8 μM fluconazole, or the combination, and growth was monitored for 48 h. Neither iron nor manganese availability significantly altered fungal growth under these treatment conditions, even when iron concentrations exceeded the prochelator concentration fourfold (Fig. 5A and B). These findings indicate that supplementation with iron or manganese does not restore growth inhibited under combined fluconazole and prochelator stress, nor does it markedly influence prochelator activity in the absence of azole.

In contrast, zinc availability had a pronounced effect on *C. albicans* growth. Under both zinc-deficient and excess conditions, growth was reduced relative to zinc-replete media (Fig. 5C). Treatment with $(AH1\text{-}S)_2$ accentuated this trend, suggesting that zinc homeostasis influences the activity of this prochelator (Fig. 5C). This zinc-dependent effect was less pronounced for

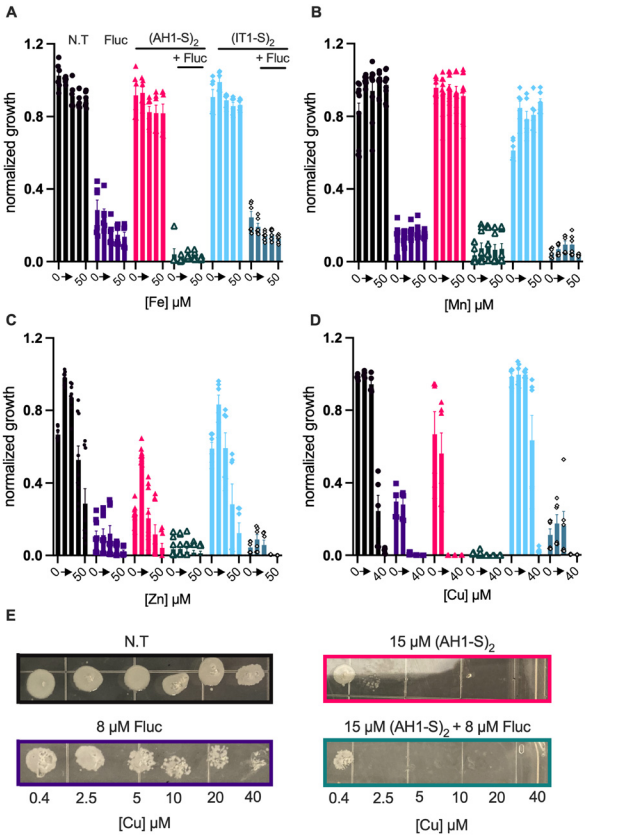

Fig. 5 (A)–(D) Metals were added into SD medium made without the designated metal to give a concentration that ranged from deficient to excess. Under these conditions, *C. albicans* SC5314 were not treated (NT, black bars, circles) or treated with 8 μM fluconazole (purple bars, squares), 15 μM $(AH1\text{-}S)_2$ (pink bars, triangles), $(IT1\text{-}S)_2$ (light blue, triangles), or combined 15 μM prochelator plus 8 μM fluconazole (green triangles or dark blue rhombus). Growth was measured by OD_{600} after 48 h and normalized relative to non-treated cells. (E) Cidality assays on YPD agar plates after 48 h. Non-toxic levels of copper convert $(AH1\text{-}S)_2$ from fungistatic to fungicidal. The images above are representative of at least n = 2 biological replicates of n = 1–3 technical replicates. Error bars represent SEM.

$(IT1\text{-}S)_2$, highlighting a divergence in how the two compounds interact with cellular metals (Fig. 5C).

Copper availability also modulated fungal growth and prochelator activity. *C. albicans* tolerated copper supplementation up to 10 μM, whereas higher concentrations were toxic under these conditions (Fig. 5D). Consistent with prior reports, non-toxic copper supplementation potentiated the antifungal activity of fluconazole by suppressing trailing growth (Fig. 5D).[17,36] Strikingly, the presence of copper also significantly enhanced the antifungal activity of $(AH1\text{-}S)_2$, with as little as 2.5 μM copper being sufficient to completely inhibit growth in the presence of the prochelator (Fig. 5D). In contrast, $(IT1\text{-}S)_2$ appeared to confer a slight protective effect against copper.

In addition to enhancing growth inhibition, copper supplementation converted $(AH1\text{-}S)_2$ treatment, either alone or in combination with fluconazole, from fungistatic to fungicidal, as assessed by post-treatment spotting assays (Fig. 5E). This copper-

dependent shift in outcome was not observed for $(IT1\text{-}S)_2$, further underscoring mechanistic differences between the two prochelators (Fig. S11).

Collectively, these results demonstrate that the activity of $(AH1\text{-}S)_2$ against *C. albicans* is influenced by extracellular metal availability, particularly zinc and copper, whereas iron and manganese have minimal impact under the conditions tested. These findings indicate that $(AH1\text{-}S)_2$ modulates fungal growth through metal-dependent mechanisms, motivating further investigation into how this prochelator perturbs intracellular metal handling under azole stress.

$(AH1\text{-}S)_2$ redistributes intracellular iron, manganese and copper under fluconazole stress

To further define how $(AH1\text{-}S)_2$ modulates metal handling in *C. albicans*, we quantified bulk cellular metal content after treatment by using inductively-plasma-coupled mass spectrometry (ICP-MS). For sufficient material for analysis, cells were grown in large cultures in nutrient-rich YPD medium and treated with fluconazole, $(AH1\text{-}S)_2$, or a combination of both for 90 min or 6 h. Given the pronounced copper-dependent effects observed in SD medium, we additionally examined the impact of copper supplementation alone and in combination with $(AH1\text{-}S)_2$.

Across all treatment conditions, total cell-associated metal content generally decreased between 90 min and 6 h (Table S2). Although zinc levels were not impacted by the treatment condition at either timepoint, iron and manganese levels were significantly changed by fluconazole and $(AH1\text{-}S)_2$ after 6 h compared to non-treated cells (Fig. 6). At 6 h, fluconazole-treated cells retained approximately twofold more iron than non-treated controls, consistent with previous reports linking azole stress to iron accumulation (Fig. 6A).[17] Treatment with $(AH1\text{-}S)_2$ alone reduced cellular iron content by ~50%. Notably, combined treatment with $(AH1\text{-}S)_2$ and fluconazole restored iron levels to those of untreated cells, indicating that the prochelator counteracts fluconazole-induced iron retention. Copper supplementation also increased iron accumulation, with combined copper and $(AH1\text{-}S)_2$ treatment producing a 1.7-fold increase of cellular iron relative to non-treated cells (Fig. 6A). These data are consistent with the known dependency of copper on iron uptake.

Similar to iron, the cellular manganese content approximately doubled after 6 h incubation with fluconazole alone but remained comparable to untreated controls for all other conditions (Fig. 6B). The fluconazole-induced retention of iron and manganese correlated with reduced growth at 6 h relative to untreated cells for this condition, whereas the combination treatment showed growth recovery comparable to untreated cells (Fig. S12). This outcome mirrors the growth behavior in checkerboard assays under concentrations of high prochelator and low azole (Fig. 4), suggesting that modulation of metal retention contributes to context-dependent growth responses.

Copper levels were markedly affected by $(AH1\text{-}S)_2$. At 90 min, copper-supplemented cells accumulated ~2-fold more copper than untreated controls, while $(AH1\text{-}S)_2$ further augmented copper accumulation by ~8.5 fold (Fig. 6D). By 6 h, copper levels remained significantly elevated under all copper-supplemented conditions, with $(AH1\text{-}S)_2$ further enhancing accumulation. These results indicate that $(AH1\text{-}S)_2$ strongly promotes copper uptake and retention in these cells.

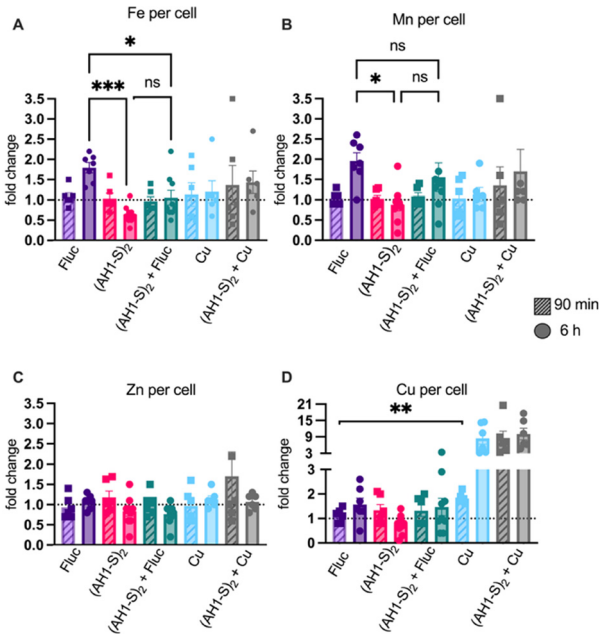

Fig. 6 Levels of (A) iron, (B) manganese, (C) zinc, and (D) copper in *C. albicans* SC5314 after 90 min and 6 h of treatment with 15 μM $(AH1\text{-}S)_2$, 10 μM fluconazole, 10 μM copper, or a combination. Data are plotted as fold change relative to the respective metal concentration for non-treated cells (represented by dashed line). Error bars represent SEM; n = 2–3 biological replicates with multiple technical replicates; at least one biological replicate performed under minimal light conditions. Welch's ANOVA p-value = 0.0001, Dunnett's T3 p-value = 0.0438 (*), 0.0075 (**), and 0.0001 (***).

Taken together, the ICP-MS data indicate that $(AH1\text{-}S)_2$ counteracts fluconazole-induced retention of iron and manganese while simultaneously promoting copper accumulation. These findings provide a mechanistic basis for the metal-dependent growth phenotypes observed in SD medium and suggest that $(AH1\text{-}S)_2$ alters intracellular metal balance rather than simply depleting total cellular iron. This conclusion motivated subsequent spectroscopic studies to probe iron speciation and directly assess the impact of $(AH1\text{-}S)_2$ on the labile iron pool.

$(AH1\text{-}S)_2$ depletes the labile iron pool through intracellular Fe(III) complex formation

Although ICP-MS provides quantitative information on bulk cellular metal content, it does not distinguish between oxidation states or intracellular speciation. In yeast, intracellular iron is distributed among cytosolic, vacuolar, and protein-bound pools. The cytosol is predominantly reducing and therefore enriched in iron(II), whereas the vacuolar or labile iron pool contains high-spin iron(III), which gives rise to a characteristic electron paramagnetic resonance (EPR) signal at $g \approx 4.3$.[17,61–63] To probe this pool directly, we performed X-band continuous-

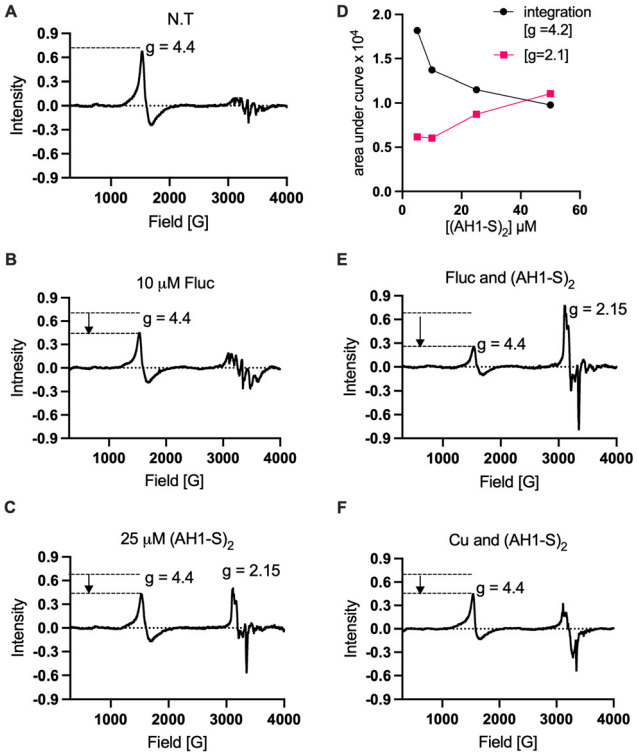

Fig. 7 (A) EPR-detectable labile iron gives a signal at g = 4.4 in non-treated (NT) cells. The intensity of g = 4.4 signal is attenuated upon treatment with (B) fluconazole or (C) $(AH1\text{-}S)_2$. $(AH1\text{-}S)_2$ treated cells also show a rhombic signal at the g = 2.15 – 2.0 region. (D) The intensity of the signals at g = 4.4 and 2.15–2.0 as a function of $[(AH1\text{-}S)_2]$. (E) $(AH1\text{-}S)_2$ and fluconazole combination attenuates the signal at g = 4.4 to a greater degree than fluconazole alone. (F) In the presence of 10 μM copper, $(AH1\text{-}S)_2$ still attenuates EPR-detectable labile iron (g = 4.4) compared to the NT control. Dashed line represents the intensity of signal at g = 4.4 for NT cells. EPR data collected at 77 K. Data shown for 6 h incubations; for additional timepoints and concentrations, see Fig. S13–S15.

wave EPR spectroscopy at 77 K on whole *C. albicans* cells treated with $(AH1\text{-}S)_2$, fluconazole, or the combination over 6 h (Fig. 7).

Non-treated cells exhibited a strong signal with g = 4.4, consistent with the presence of vacuolar high-spin iron(III) (Fig. 7A). Fluconazole treatment for 6 h decreased the intensity of this signal, consistent with previous reports (Fig. 7B).[17] Treatment with $(AH1\text{-}S)_2$ alone similarly decreased intensity of the g = 4.4 signal over the same time frame (Fig. 7C), indicating depletion of the labile iron pool. Concomitant with the loss of the high-spin iron(III) signal, new rhombic EPR features emerged with g values near 2.15, 2.10, and 2.00. These signals match previously reported spectra for low-spin Fe(III) complexes of AH1, which have been characterized in multiple protonation states.[56] The appearance of these signals within 45 min of treatment, and their increase with higher concentrations of added prochelator (Fig. 7D and Fig. S13–S14), is consistent with intracellular formation of a low-spin Fe(III)–AH1 complex with a 2 : 1 ligand-to-metal stoichiometry.[56] Combined treatment with fluconazole and $(AH1\text{-}S)_2$ further suppressed the signal at g = 4.4 compared to either treatment alone at 6 h (Fig. 7E), indicating enhanced depletion of the labile iron pool under dual stress. At an earlier 90 min time point, neither fluconazole, $(AH1\text{-}S)_2$, nor the combination significantly altered the intensity of the g = 4.4 signal (Fig. S13–S15), suggesting that redistribution or chelation of labile iron occurs on a longer time scale.

Given the pronounced effects of copper observed in growth assays and ICP-MS experiments, we also examined iron speciation under copper-supplemented conditions. Cells treated with copper alone did not exhibit depletion of the labile iron pool (Fig. S15). In contrast, cells co-treated with copper and $(AH1\text{-}S)_2$ still showed a reduction in the g = 4.4 signal (Fig. 7F), indicating that $(AH1\text{-}S)_2$ leads to depletion of labile iron even in the presence of elevated copper. Although formation of intracellular Fe(III)–AH1 complexes remains likely under these conditions, the signal is not as clearly defined and the presence of Cu–AH1 species cannot be ruled out (Fig. 7F).

Taken together, the EPR data demonstrate that $(AH1\text{-}S)_2$ depletes the labile iron(III) pool in *C. albicans* through formation of intracellular iron–chelator complexes. When considered alongside the ICP-MS results, these findings indicate that $(AH1\text{-}S)_2$ does not simply diminish total cellular iron content but rather redistributes bioavailable pools of iron while counteracting fluconazole-induced iron retention. This iron-dependent perturbation provides a mechanistic basis for the variable growth phenotypes observed under azole stress.

$(AH1\text{-}S)_2$ shows context-dependent effects in macrophage co-culture

Because $(AH1\text{-}S)_2$ targets metal-dependent vulnerabilities that are likely to be influenced by host-mediated metal processing, we next evaluated its antifungal activity in a co-culture model of *C. albicans* with macrophage-like cells. *C. albicans* SC5314 were grown either alone (mono-culture) or in the presence of J774A.1 murine macrophage-like cells (co-culture) and treated with $(AH1\text{-}S)_2$, fluconazole, or a combination of both. Treatment efficacy was evaluated by quantifying colony forming units (CFU) of *C. albicans* and assessing macrophage cytotoxicity *via* a lactate dehydrogenase (LDH) release assay.

In co-culture, the presence of activated macrophages alone reduced *C. albicans* CFUs to approximately 43% relative to fungal mono-cultures grown under the same DMEM conditions (Fig. 8A), consistent with macrophage-mediated restriction of fungal growth. Addition of a low concentration of 1.5 μM $(AH1\text{-}S)_2$ further decreased CFUs, suggesting that the prochelator can enhance antifungal pressure under these conditions. However, increasing the concentration of $(AH1\text{-}S)_2$ to 25 μM caused CFUs to rebound to levels above the no-treatment condition. This biphasic response mirrors trends observed in mono-cultures of *C. albicans* grown in DMEM, where low concentrations of $(AH1\text{-}S)_2$ inhibited growth while higher concentrations promoted growth (Fig. S16–S17). These outcomes differ from those observed in SD medium, in which increasing $(AH1\text{-}S)_2$ concentration correlated with progressively greater growth inhibition (Fig. 3), underscoring the strong influence of media composition on prochelator activity and fungal response.

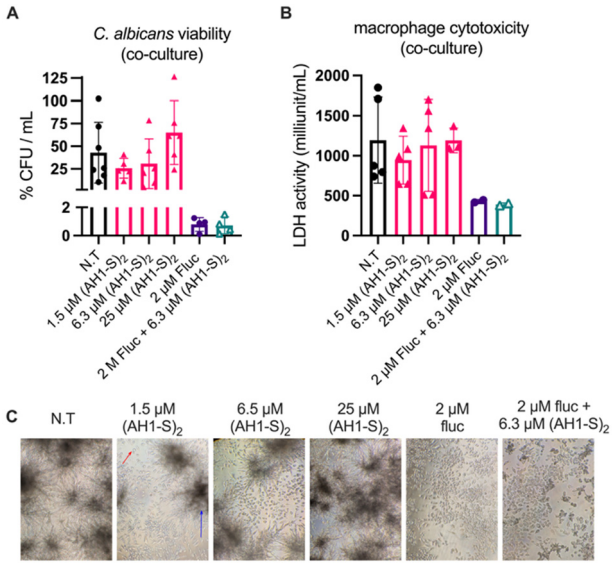

Fig. 8 (A) Percent colony forming units (CFUs)/mL of *C. albicans* SC5314 co-cultured with macrophages relative to the CFU/mL of the non-treated mono-culture. (B) Macrophage cytotoxicity as measured by LDH assay. (C) Images of cells in 96-well plates under co-culture conditions. Left to right: NT, 1.5 μM $(AH1\text{-}S)_2$, 6.5 μM $(AH1\text{-}S)_2$, 25 μM $(AH1\text{-}S)_2$, 2 μM fluconazole, and 2 μM fluconazole + 6.5 μM $(AH1\text{-}S)_2$. Cells were grown in DMEM under mammalian cell culture conditions. Red arrow – macrophage; blue arrow – *C. albicans* hyphae.

In contrast to the context dependent effects observed for $(AH1\text{-}S)_2$, fluconazole treatment (2 μM) was highly effective in co-culture, resulting in a ~99% reduction in fungal CFUs, with no additional reduction observed upon co-treatment with $(AH1\text{-}S)_2$ (Fig. 8A and C). The reduced fungal burden under fluconazole treatment correlated with decreased release of LDH by the macrophages, indicating reduced macrophage damage under these conditions (Fig. 8B). Treatment in co-culture with $(AH1\text{-}S)_2$ alone did not significantly alter macrophage LDH activity relative to untreated co-culture controls. However, exposure of macrophages in mono-culture to $(AH1\text{-}S)_2$ concentrations above 12.5 μM resulted in elevated LDH release (Fig. S16), indicative of compromised macrophage membrane integrity. These findings suggest that higher concentrations of $(AH1\text{-}S)_2$ exert cytotoxic effects on macrophages, which may indirectly contribute to the enhanced fungal growth observed at elevated prochelator concentrations in co-culture.

Taken together, these results indicate that while low concentrations of $(AH1\text{-}S)_2$ can modestly reduce fungal burden in the presence of macrophages, higher concentrations provide a growth advantage to *C. albicans*, potentially through adverse effects on macrophage viability.

Conclusions

This study demonstrates that a thiol-activated prochelation strategy can enhance antifungal activity by exploiting metal-dependent vulnerabilities in *C. albicans*. Our findings reveal that select prochelators modulate fungal growth under azole stress in a metal-dependent manner, with outcomes influenced by both the specific prochelator, the degree of azole stress, and media composition. Notably, $(AH1\text{-}S)_2$ prevents bulk iron accumulation under fluconazole exposure by reducing labile iron through intracellular iron–chelator complex formation. Beyond its direct effect on iron, $(AH1\text{-}S)_2$ promotes copper accumulation under otherwise non-toxic copper conditions, a phenomenon that contributes to fungicidal activity. An important question for future investigation is whether this phenotypic response reflects direct complex formation between copper and the prochelator or chelator, or instead arises from indirect effects of copper availability.

The activity of $(AH1\text{-}S)_2$ is noticeably influenced by its environmental context. In the Synthetic Defined fungal media, copper and zinc availability shape growth outcomes, whereas iron and manganese supplementation have minimal impact under the conditions tested. In contrast, co-culture experiments reveal that host-pathogen interactions impose additional constraints: while low concentrations of $(AH1\text{-}S)_2$ modestly reduce fungal burden in the presence of macrophages, higher concentrations compromise macrophage viability and nullify antifungal benefit. These results highlight a loss of fungal selectivity at elevated prochelator concentrations, suggesting that targeted fungal selectivity could improve outcomes. Future work will focus on improving fungal specificity and elucidating the mechanistic basis of copper accumulation and cidality to fully harness this approach for therapeutic development.

Experimental

Yeast strains, culture media, and stock solutions

Candida albicans laboratory strain SC5314 (MYA 28776), purchased from ATCC, was used for all experiments unless otherwise noted. *Candida albicans* fluconazole-resistant Y172 strain is a clinical isolate generously provided by the Alspaugh lab at Duke University. Cells were stored at −80 °C in 15–20% glycerol. Broth microdilution assays were conducted in 0.165 M MOPS buffered Synthetic Defined (SD) medium pH 6.9 prepared in house to rigorously control the metal content (See Supplemental Information Table S1). For metal-add back experiments, *C. albicans* were cultured in SD medium lacking the indicated metal. Metals were reintroduced by serial dilution in 96 well plates from ~100 mM metal stock solutions of iron(III) chloride, copper(II) sulfate, manganese(II) chloride, or zinc(II) sulfate.

For EPR and ICP-MS samples, cells were grown in Yeast Peptone Dextrose (YPD) medium (Gibco). J774A.1 murine BALB/c immortalized macrophage cells derived from reticulum cell sarcoma (ATCC, TIB-67) were used for co-culture experiments with *C. albicans.* Macrophages were grown in Dulbecco's Modified Eagle Medium (DMEM) (Gibco, catalog #31053-028) without phenol red. DMEM was supplemented with 1% bovine serum (Gibco, catalog#1140-050), 1 mM sodium pyruvate (Gibco, catalog#11360-070), and 1× penicillin–streptomycin (Gibco, catalog #15140122). Macrophages were passaged every 3–4 days and discarded after ~25 passages.

100 mM stock solutions of fluconazole (Acros), voriconazole (TCI), clotrimazole, and econazole (Thermo Scientific) were prepared in DMSO and stored in aliquots at −20 °C.

Cellular growth assays

Two-dimensional microdilution assays: To examine the combined impact of prochelators and azoles on *C. albicans* growth, two-dimensional broth microdilution (checkerboard) assays were performed. *C. albicans* from frozen glycerol stocks were streaked onto YPD agar plates and incubated at 30 °C for 22–24 h. Overnight cultures were prepared by inoculating one to three colonies into 5 mL of SD medium and incubating at 30 °C with shaking (200 rpm). The following day, working solutions of azoles (1 mM in SD) and prochelators (1 or 5 mM in DMSO) were used to prepare solutions in SD of 20× and 5× the final concentration, respectively. Cell suspensions were prepared by diluting overnight cultures to an OD_{600} of 0.001, and 150 μL was added to each inner well of a 96 well plate. Prochelators (40 μL of 5 × solutions) and azoles (10 μL of 20× solutions) were added to achieve a final volume of 200 μL per well, with final concentrations ranging from 0–25 μM prochelator and 0–8 μM azole. Plates were incubated at 30 °C with shaking (200 rpm), and growth was monitored by OD_{600} at 0, 24, and 48 h. Cell growth was normalized to the average OD_{600} for the untreated control per biological replicate. For experiments with $(AH1\text{-}S)_2$, at least one biological replicate was performed under minimal light conditions, although control experiments revealed little difference in growth inhibitory effect under ambient light conditions vs strict darkness (Fig. S7). Final DMSO concentrations did not exceed 1%. After the final time point at 48 h, cidality was assessed by spotting 3 μL aliquots from each well of the 96 well plate onto YPD agar. Plates were incubated for 16–18 h at 30 °C and examined visually for colony formation.

C. albicans, *macrophage co-culture experiments*: On day 0, macrophages were seeded into 2 tissue-cultured treated 96 well plates in 100 μL of DMEM at a density of 1×10^5 viable cells per mL and incubated for 24 h at 37 °C and 5% CO_2. One colony of *C. albicans* from a YPD agar plate was used to inoculate 5 mL of YPD medium which was incubated at 30 °C and 200 rpm for 16–18 h. On day 1, macrophage culture media were aspirated and replaced with 100 μL of fresh, pre-warmed DMEM containing 10 nM phorbol myristate acetate (PMA). To activate macrophages, plates were incubated at 37 °C with 5% CO_2 for 1 h. *C. albicans* were removed from the incubator and washed twice with phosphate buffer saline (PBS) by centrifuging at 3000× *g*, 4 °C for 5 min. Fungal cells were then resuspended in DMEM, counted, and kept on ice until use. Following macrophage activation, one 96-well plate was maintained as a macrophage-only control, with 96 μL of DMEM added to each well. A second plate served as the experimental co-culture plate, to which 94 μL of DMEM was added per well. A third plate containing fungal monocultures received 194 μL of DMEM per well. *C. albicans* were added to plates 2 and 3 at a volume of 2 μL such that the final cell count was 1×10^5 cells per mL per well. Next, aliquots of copper or fluconazole at a concentration 100× the final were serially diluted two-fold down column 12, and 2 μL were added to each inner well so the final concentration for copper was 0–50 μM or 0–13 μM and fluconazole was 0–2 μM. In row H, $(AH1\text{-}S)_2$ was serially diluted across the row at 100× the final of 0–25 μM or 0–6.5 μM when 2 μL were added to each inner well. DMSO concentration was kept below 0.25%. All plates were incubated at 37 °C, 5% CO_2 for 24 h.

On day 2, fungal-macrophage interactions were visualized on a VWR VistaVision light microscope with 10× magnification and images were captured using a Google Pixel 7 with 3× zoom. Macrophage cell viability was determined using a lactate dehydrogenase (LDH) release assay kit (Abcam, catalog #AB102526). NADH standards (50 μL) were prepared in concentrations ranging from 0–0.5 nmol/well from a 1.25 mM stock. A 5 μL portion of spent media was added to 45 μL LDH buffer, followed by the addition of 50 μL of LDH substrate mix. The degree of NADH oxidation was monitored over 30 min by absorption at 450 nm using a PerkinElmer Victor3 V plate reader preheated to 37 °C. LDH activity was quantified using the following equation:

$$\text{LDH activity} = \left(\frac{B}{\Delta T \times V}\right) \times D$$

where B is the amount of NADH/well calculated from the NADH standard curve, ΔT is reaction time, V is original sample volume added into the reaction well in mL, and D is sample dilution. Fungal viability was determined by calculating colony forming units (CFUs). Percent growth reduction was calculated according to the equation below:

$$\%\text{Growth} = \frac{(\text{CFU}_{\text{N.T.mean}} - \text{CFU}_{\text{treatment.mean}})}{\text{CFU}_{\text{N.T.mean}}}$$

Select treatment conditions were chosen based on microscopy, and cells were diluted in PBS between 1 : 10 and 1 : 10 000. 100 μL of diluted cells were spread onto YPD agar plates using colirollers plating beads (VWR, catalog # EM71013-3). Plates were incubated at 30 °C for ∼ 24 h and the number of colonies were counted.

UV-visible spectroscopy

The stability of compounds in solution was examined by UV-visible spectroscopy. Spectra were collected from 230 nm to 800 nm over 8 h on a Varian Cary 50 UV-visible spectrophotometer in quartz cuvettes with 10 mm pathlength. Samples consisted of 2-mL solutions of prochelator (15 μM), prepared from a 20 mM DMSO stock solution in either SD medium or 0.165 M MOPS buffer (pH 6.9). Final DMSO concentrations did not exceed 1%.

Mass spectrometry

Solutions (5 mL) of 15 μM $(AH1\text{-}S)_2$, 5.5 μM riboflavin or both were prepared in 0.165 M MOPS buffer (pH 6.9) in Eppendorf tubes that were either exposed to ambient light or wrapped in aluminum foil to minimize light exposure. Aliquots were analyzed by LC-MS immediately after preparation and again after 8 h and 24 h. LC-MS data were collected on an Agilent 6460

Triple Quadrupole LC-MS equipped with a Kinetex EVO C18 column (100 × 3.0 mm, 2.6 μm). For chromatographic separation, the mobile phase gradient was 100% of 100 : 3 : 0.3 water:methanol:formic acid to 100% of 100 : 3 : 0.3 acetonitrile:water:formic acid over 8 min. Samples were detected by UV-vis absorbance *via* photodiode array detector (DAD) from 200 to 800 nm, and by electrospray ionization (ESI) using positive polarity.

EPR and ICP-MS

For EPR and ICP-MS samples, multiple (5–10×) overnight cultures were prepared from 1–3 colonies and grown overnight (~16–22 h) in 5 mL of YPD media at 30 °C shaking at 200 rpm. The following day, the cultures were combined then diluted into YPD to make a culture between 425–1000 mL with an initial OD_{600} of 0.3. These cultures were split into multiple flasks to allow for appropriate aeration, then incubated at 30 °C and 200 rpm until the cells had entered exponential growth (OD_{600} between 0.35–0.5). The culture was recombined, then split into subcultures for treatment with 25 μM $(AH1\text{-}S)_2$, 10 μM fluconazole, 10 μM $CuCl_2$, or a combination. A range of 0–50 μM $(AH1\text{-}S)_2$ was also evaluated.

For EPR, cells were incubated after treatment at 30 °C and 200 rpm for up to 6 h. At the desired timepoint, the OD_{600} value was recorded, and 2×10^9 cells were harvested based on an experimentally determined cell density of OD_{600} 1.0 = 3×10^7 cells. Cells were pelleted, washed with 5 mM EDTA to remove extracellular metals, then washed with 20 mM Tris-HCl, pH 7.6. Pellets were resuspended in 300 μL of 20 mM Tris-HCl, pH 7.4 + 20% glycerol. The cell suspensions were flash-frozen in liquid nitrogen and stored at −80 °C.

X-band continuous wave EPR spectroscopy was performed on a Bruker ESP 300 spectrometer equipped with an Oxford Instruments ESR 910 continuous helium flow cryostat. Experiments were conducted at 77 ± 1 K, 20 mW microwave power, and 5 G modulation amplitude. Samples were baselined followed by a double integration on the Bruker EPR software. Easyspin was used to fit the spectra and define *g* values.

For ICP-MS, cells were incubated at 30 °C and 200 rpm for either 90 min or 6 h. At time of harvest, the OD_{600} was recorded and the culture was pelleted at 4000 × *g* for 10 min and washed with 5 mM EDTA. The pellets were dried overnight at ~ 90 °C. Dried pellets were lysed by adding 100 μL of concentrated, trace metal grade nitric acid (Fischer Scientific) and were incubated at 90 °C for ~2 h. Lysed cells were diluted by adding 900 μL of 1% nitric acid. Samples were stored at −20 °C until use. Samples were prepared in 2–3 biological replicates, each containing 1–3 technical replicates. These samples were diluted into a solution of 2% (v/v) trace metal grade nitric acid with 0.5% (v/v) trace metal grade hydrochloric acid spiked with 20 ppb ^{72}Ge, ^{89}Y, ^{115}In as internal standards. Samples were run on an Agilent 7900 ICP-MS (Agilent Technologies, Santa Clara, CA, USA), in He mode or H_2 mode to reduce polyatomic interferences. Copper, manganese, and zinc were measured under a He atmosphere (collision cell) with a He gas flow rate of 5 mL min^{-1}, and iron was measured under a H_2 atmosphere with a flow rate of 6 mL min^{-1} H_2 gas. Data were quantified using weighed, serial dilutions of multi-element standards (SPEX CertiPrep, CLMS-2AN). A premixed drinking water standard (CRMTDWA from High Purity Standards) was used as an initial calibration verification and kept within ± 10% of the expected value. Internal standards ^{72}Ge, ^{89}Y, and ^{115}In were kept within ±10% of the expected value. The quantified values were the average of seven replicates.

Concentrations of iron, copper, zinc, or manganese were converted from parts per billion (ppb) to μM by dividing each metal by its respective molar mass. Data were normalized per cell by dividing the total μM by the cell per mL count (OD_{600} 1.0 = 3×10^7 cells) and reported as fold change and in units of μmol metal/cell. Significance was determined using a Brown Forsythe and Welch Analysis of Variance (ANOVA) test followed by a Dunnet T3 multiple comparison test on GraphPad Prism software. Error bars represent the standard error of the mean (SEM).

Author contributions

MAM.: conceptualization; investigation; visualization; methodology; writing – original draft; writing review and editing. CADJ: conceptualization; investigation; methodology; writing-review and editing. FV: investigation; methodology; writing – review and editing. ABH: Investigation. YS: Resources. ET: conceptualization; funding acquisition; writing – review and editing. KJF: conceptualization; funding acquisition; writing – original draft; writing – review and editing; project administration; supervision.

Conflicts of interest

There are no conflicts to declare.

Abbreviations

CFU	colony forming units
EPR	electron paramagnetic resonance spectroscopy
Fluc	fluconazole
ICP-MS	inductively-coupled plasma mass spectrometry
LDH	lactate dehydrogenase
MOPS	4-morpholinepropanesulfonic acid
NT	not treated
OD_{600}	optical density at 600 nm
ROS	reactive oxygen species
SEM	standard error of mean
SD	synthetic defined medium
YPD	yeast peptone dextrose medium

Data availability

Data supporting this article are included in the supplementary information (SI). Supplementary information includes

additional spectra, growth assays, media components, and images. See DOI: https://doi.org/10.1039/d6cb00073h.

Acknowledgements

This work was supported in part with funds from the National Institutes of Health (grant R01GM084176 to KJF and grant R35 GM153364 to ET). KJF also acknowledges support as a Marcil-Monahan Scholar of Trinity College of Arts and Sciences, Duke University. We acknowledge fellowship support from the Tri-Institutional Molecular Mycology and Pathogenesis Training Program (NIH T21-AI052080, for CADJ and FAV), and NIH F32 (F32GM153029) for FAV. We thank Duke's Office of Undergraduate Research Support for grants to A.B. We thank Prof. Kenichi Yokoyama and Duke Biochemistry for training and access to the X-band EPR spectrometer, which was funded by an Institutional Development Grant (ID2014-IDG-1017) from the North Carolina Biotechnology Center. We thank Dr. Nelson Rivera and the Hsu-Kim lab for training and access to the ICP-MS housed in the Pratt Trace Element Analysis Service Center at Duke University. We thank the Alspaugh lab at Duke University for access to the *C. albicans* clinical isolate Y172.

References

1 M. Giannella, F. Lanternier, S. Dellière, A. H. Groll, N. J. Mueller, A. Alastruey-Izquierdo and M. A. Slavin, Invasive fungal disease in the immunocompromised host: changing epidemiology, new antifungal therapies, and management challenges, *Clin. Microbiol. Infect.*, 2025, **31**, 29–36.
2 D. W. Denning, Global incidence and mortality of severe fungal disease, *Lancet Infect. Dis.*, 2024, **24**, e428–e438.
3 G. R. Thompson and A. N. Desai, Addressing Antifungal Drug Resistance—A ''One Health–One World'' Challenge, *N. Engl. J. Med.*, 2025, **392**, 2187–2189.
4 I. D. Iliev, G. D. Brown, P. Bacher, S. L. Gaffen, J. Heitman, B. S. Klein and M. S. Lionakis, Focus on fungi, *Cell*, 2024, **187**, 5121–5127.
5 M. Hoenigl, R. Sprute, M. Egger, A. Arastehfar, O. A. Cornely, R. Krause, C. Lass-Flörl, J. Prattes, A. Spec, G. R. Thompson 3rd, N. Wiederhold and J. D. Jenks, The Antifungal Pipeline: Fosmanogepix, Ibrexafungerp, Olorofim, Opelconazole, and Rezafungin, *Drugs*, 2021, **81**, 1703–1729.
6 L. Kriegl, M. Egger, J. Boyer, M. Hoenigl and R. Krause, New treatment options for critically important WHO fungal priority pathogens, *Clin. Microbiol. Infect.*, 2025, **31**, 922–930.
7 A. A. Sagatova, M. V. Keniya, R. K. Wilson, B. C. Monk and J. D. A. Tyndall, Structural Insights into Binding of the Antifungal Drug Fluconazole to Saccharomyces cerevisiae Lanosterol-14α-Demethylase, *Antimicrob. Agents Chemother.*, 2015, **59**, 4982–4989.
8 Y. Aoyama, Y. Yoshida and R. Sato, Yeast cytochrome P-450 catalyzing lanosterol 14 alpha-demethylation. II. Lanosterol metabolism by purified P-450(14)DM and by intact microsomes, *J. Biol. Chem.*, 1984, **259**, 1661–1666.
9 A. Kane and D. A. Carter, Augmenting Azoles with Drug Synergy to Expand the Antifungal Toolbox, *Pharmaceuticals*, 2022, **15**, 482.
10 R. Prasad, P. De Wergifosse, A. Goffeau and E. Balzi, Molecular cloning and characterization of a novel gene of Candida albicans, CDR1, conferring multiple resistance to drugs and antifungals, *Curr. Genet.*, 1995, **27**, 320–329.
11 M. L. Hernáez, C. Gil, J. Pla and C. Nombela, Induced expression of the Candida albicans multidrug resistance gene CDR1 in response to fluconazole and other antifungals, *Yeast*, 1998, **14**, 517–526.
12 A. R. Holmes, T. S. Cardno, J. J. Strouse, I. Ivnitski-Steele, M. V. Keniya, K. Lackovic, B. C. Monk, L. A. Sklar and R. D. Cannon, Targeting Efflux Pumps to Overcome Antifungal Drug Resistance, *Future Med. Chem.*, 2016, **8**, 1485–1501.
13 S. Perea, J. L. López-Ribot, W. R. Kirkpatrick, R. K. McAtee, R. A. Santillán, M. Martínez, D. Calabrese, D. Sanglard and T. F. Patterson, Prevalence of molecular mechanisms of resistance to azole antifungal agents in Candida albicans strains displaying high-level fluconazole resistance isolated from human immunodeficiency virus-infected patients, *Antimicrob. Agents Chemother.*, 2001, **45**, 2676–2684.
14 R. Franz, S. L. Kelly, D. C. Lamb, D. E. Kelly, M. Ruhnke and J. Morschhäuser, Multiple molecular mechanisms contribute to a stepwise development of fluconazole resistance in clinical Candida albicans strains, *Antimicrob. Agents Chemother.*, 1998, **42**, 3065–3072.
15 T. Prasad, A. Chandra, C. K. Mukhopadhyay and R. Prasad, Unexpected Link between Iron and Drug Resistance of *Candida* spp.: Iron Depletion Enhances Membrane Fluidity and Drug Diffusion, Leading to Drug-Susceptible Cells, *Antimicrob. Agents Chemother.*, 2006, **50**, 3597–3606.
16 A. Tripathi, E. Liverani, A. Y. Tsygankov and S. Puri, Iron alters the cell wall composition and intracellular lactate to affect Candida albicans susceptibility to antifungals and host immune response, *J. Biol. Chem.*, 2020, **295**, 10032–10044.
17 E. W. Hunsaker and K. J. Franz, Candida albicans reprioritizes metal handling during fluconazole stress, *Metallomics*, 2019, **11**, 2020–2032.
18 R. Sharma, A. Nahar and S. Puri, Candida albicans enhances iron uptake to maintain fluconazole resistance, *Infect. Immun.*, 2025, **93**, e0000225.
19 I. Khemiri, F. Tebbji, A. Burgain and A. Sellam, Regulation of copper uptake by the SWI/SNF chromatin remodeling complex in Candida albicans affects susceptibility to antifungal and oxidative stresses under hypoxia, *FEMS Yeast Res.*, 2024, 24.
20 E. W. Hunsaker, C. A. Yu and K. J. Franz, Copper Availability Influences the Transcriptomic Response of Candida albicans to Fluconazole Stress, *G3*, 2021, **11**(4), jkab065.
21 M. G. Netea, L. A. Joosten, J. W. van der Meer, B. J. Kullberg and F. L. van de Veerdonk, Immune defence against Candida fungal infections, *Nat. Rev. Immunol.*, 2015, **15**, 630–642.

22 J. Potrykus, E. R. Ballou, D. S. Childers and A. J. Brown, Conflicting interests in the pathogen-host tug of war: fungal micronutrient scavenging versus mammalian nutritional immunity, *PLoS Pathog.*, 2014, **10**, e1003910.
23 T. Ganz, Macrophages and Iron Metabolism, *Microbiol. Spectrum*, 2016, **4**(5), DOI: 10.1128/microbiolspec.mchd-0037-2016.
24 S. García-Santamarina and D. J. Thiele, Copper at the Fungal Pathogen-Host Axis*, *J. Biol. Chem.*, 2015, **290**, 18945–18953.
25 B. A. Gingras, G. Colin and C. H. Bayley, Antifungal Activity of Thiosemicarbazones, *J. Pharmacol. Sci.*, 1965, **54**, 1674–1675.
26 Y. W. Lai, L. T. Campbell, M. R. Wilkins, C. N. Pang, S. Chen and D. A. Carter, Synergy and antagonism between iron chelators and antifungal drugs in Cryptococcus, *Int. J. Antimicrob. Agents*, 2016, **48**, 388–394.
27 V. Opletalova, D. S. Kalinowski, M. Vejsova, J. Kunes, M. Pour, J. Jampilek, V. Buchta and D. R. Richardson, Identification and characterization of thiosemicarbazones with antifungal and antitumor effects: cellular iron chelation mediating cytotoxic activity, *Chem. Res. Toxicol.*, 2008, **21**, 1878–1889.
28 M. T. C. Ang, R. Gumbau-Brisa, D. S. Allan, R. McDonald, M. J. Ferguson, B. E. Holbein and M. Bierenstiel, DIBI, a 3-hydroxypyridin-4-one chelator iron-binding polymer with enhanced antimicrobial activity, *MedChemComm*, 2018, **9**, 1206–1212.
29 K. A. Savage, M. C. Parquet, D. S. Allan, R. J. Davidson, B. E. Holbein, E. A. Lilly and P. L. Fidel, Jr., Iron Restriction to Clinical Isolates of Candida albicans by the Novel Chelator DIBI Inhibits Growth and Increases Sensitivity to Azoles In Vitro and In Vivo in a Murine Model of Experimental Vaginitis, *Antimicrob. Agents Chemother.*, 2018, **62**(8), DOI: 10.1128/aac.02576-17.
30 X. Jiang, T. Zhou, R. Bai and Y. Xie, Hydroxypyridinone-Based Iron Chelators with Broad-Ranging Biological Activities, *J. Med. Chem.*, 2020, **63**, 14470–14501.
31 X. Duan, Z. Xie, L. Ma, X. Jin, M. Zhang, Y. Xu, Y. Liu, H. Lou and W. Chang, Selective Metal Chelation by a Thiosemicarbazone Derivative Interferes with Mitochondrial Respiration and Ribosome Biogenesis in Candida albicans, *Microbiol. Spectrum*, 2022, **10**(3), e01951–21.
32 S. Fallah, D. Duncan, K. D. Reichl, M. J. Smith, W. Wang, J. A. Porco, Jr., L. E. Brown, L. Whitesell, N. Robbins and L. E. Cowen, A chemical screen identifies structurally diverse metal chelators with activity against the fungal pathogen Candida albicans, *Microbiol. Spectrum*, 2024, **12**(4), e04095–23.
33 J. Qian, N. P. Wiederhold, T. Patterson, H. Patterson and C. J. Berkland, Polymeric Iron Chelator with Enhanced Iron Affinity as a Broad-Spectrum Antifungal Agent, *ACS Appl. Polym. Mater.*, 2021, **3**, 6034–6039.
34 B. E. Holbein and R. Mira de Orduña, Effect of trace iron levels and iron withdrawal by chelation on the growth of Candida albicans and Candida vini, *FEMS Microbiol. Lett.*, 2010, **307**, 19–24.
35 R. A. Festa, M. E. Helsel, K. J. Franz and D. J. Thiele, Exploiting Innate Immune Cell Activation of a Copper-Dependent Antimicrobial Agent during Infection, *Chem. Biol.*, 2014, **21**, 977–987.
36 E. W. Hunsaker and K. J. Franz, Copper potentiates azole antifungal activity in a way that does not involve complex formation, *Dalton Trans.*, 2019, **48**, 9654–9662.
37 M. E. Helsel, E. J. White, S. Z. A. Razvi, B. Alies and K. J. Franz, Chemical and functional properties of metal chelators that mobilize copper to elicit fungal killing of Cryptococcus neoformans†, *Metallomics*, 2016, **9**, 69–81.
38 N. L. Reeder, J. Kaplan, J. Xu, R. S. Youngquist, J. Wallace, P. Hu, K. D. Juhlin, J. R. Schwartz, R. A. Grant, A. Fieno, S. Nemeth, T. Reichling, J. P. Tiesman, T. Mills, M. Steinke, S. L. Wang and C. W. Saunders, Zinc Pyrithione Inhibits Yeast Growth through Copper Influx and Inactivation of Iron-Sulfur Proteins, *Antimicrob. Agents Chemother.*, 2011, **55**, 5753–5760.
39 N. L. Stevanović, I. Aleksic, J. Kljun, S. Skaro Bogojevic, A. Veselinovic, J. Nikodinovic-Runic, I. Turel, M. I. Djuran and B. Đ. Glišić, Copper(II) and Zinc(II) Complexes with the Clinically Used Fluconazole: Comparison of Antifungal Activity and Therapeutic Potential, *Pharmaceuticals*, 2021, **14**, 24.
40 Q. Wang and K. J. Franz, Stimulus-Responsive Prochelators for Manipulating Cellular Metals, *Acc. Chem. Res.*, 2016, **49**, 2468–2477.
41 E. W. Hunsaker and K. J. Franz, Emerging Opportunities To Manipulate Metal Trafficking for Therapeutic Benefit, *Inorg. Chem.*, 2019, **58**, 13528–13545.
42 V. Oliveri, Selective Targeting of Cancer Cells by Copper Ionophores: An Overview, *Front. Mol. Biosci.*, 2022, **9**, 841814.
43 E. Saxon and X. Peng, Recent Advances in Hydrogen Peroxide Responsive Organoborons for Biological and Biomedical Applications, *ChemBioChem*, 2022, **23**, e202100366.
44 G. Centola, F. Xue and A. Wilks, Metallotherapeutics development in the age of iron-clad bacteria, *Metallomics*, 2020, **12**, 1863–1877.
45 A. Steinbrueck, A. C. Sedgwick, J. T. Brewster, K.-C. Yan, Y. Shang, D. M. Knoll, G. I. Vargas-Zúñiga, X.-P. He, H. Tian and J. L. Sessler, Transition metal chelators, pro-chelators, and ionophores as small molecule cancer chemotherapeutic agents, *Chem. Soc. Rev.*, 2020, **49**, 3726–3747.
46 M. J. Patterson, C. G. McKenzie, D. A. Smith, A. da Silva Dantas, S. Sherston, E. A. Veal, B. A. Morgan, D. M. MacCallum, L.-P. Erwig and J. Quinn, Ybp1 and Gpx3 Signaling in Candida albicans Govern Hydrogen Peroxide-Induced Oxidation of the Cap1 Transcription Factor and Macrophage Escape, *Antioxid. Redox Signaling*, 2013, **19**, 2244–2260.
47 P. Miramón, C. Dunker, L. Kasper, I. D. Jacobsen, D. Barz, O. Kurzai and B. Hube, A family of glutathione peroxidases contributes to oxidative stress resistance in Candida albicans, *Med. Mycol.*, 2014, **52**, 223–239.
48 S. H. Lee, S. C. Chung, J. Shin and K. B. Oh, GST2 is required for nitrogen starvation-induced filamentous growth in Candida albicans, *J. Microbiol. Biotechnol.*, 2014, **24**, 1207–1215.

49 A. T. Tillmann, K. Strijbis, G. Cameron, E. Radmaneshfar, M. Thiel, C. A. Munro, D. M. MacCallum, B. Distel, N. A. R. Gow and A. J. P. Brown, Contribution of Fdh3 and Glr1 to Glutathione Redox State, Stress Adaptation and Virulence in Candida albicans, *PLoS One*, 2015, **10**, e0126940.

50 T. Wangsanut and M. Pongpom, The Role of the Glutathione System in Stress Adaptation, Morphogenesis and Virulence of Pathogenic Fungi, *Int. J. Mol. Sci.*, 2022, **23**, 10645.

51 B. Black, L. B. R. da Silva, G. Hu, X. Qu, D. F. Q. Smith, A. A. Magaña, L. C. Horianopoulos, M. Caza, R. Attarian, L. J. Foster, A. Casadevall and J. W. Kronstad, Glutathione-mediated redox regulation in Cryptococcus neoformans impacts virulence, *Nat. Microbiol.*, 2024, **9**, 2084–2098.

52 E. A. Veal, W. M. Toone, N. Jones and B. A. Morgan, Distinct Roles for Glutathione S-Transferases in the Oxidative Stress Response in Schizosaccharomyces pombe*, *J. Biol. Chem.*, 2002, **277**, 35523–35531.

53 B. Maras, L. Angiolella, G. Mignogna, E. Vavala, A. Macone, M. Colone, G. Pitari, A. Stringaro, S. Dupré and A. T. Palamara, Glutathione metabolism in Candida albicans resistant strains to fluconazole and micafungin, *PLoS One*, 2014, **9**, e98387.

54 T. M. Chang and E. Tomat, Disulfide/thiol switches in thiosemicarbazone ligands for redox-directed iron chelation, *Dalton Trans.*, 2013, **42**, 7846–7849.

55 Y. S. Sung, W. Wu, M. A. Ewbank, R. D. Utterback, M. T. Marty and E. Tomat, Albumin Conjugates of Thiosemicarbazone and Imidazole-2-thione Prochelators: Iron Coordination and Antiproliferative Activity, *ChemMedChem*, 2021, **16**, 2764–2768.

56 A. V. Astashkin, R. D. Utterback, Y.-S. Sung and E. Tomat, Iron Complexes of an Antiproliferative Aroyl Hydrazone: Characterization of Three Protonation States by Electron Paramagnetic Resonance Methods, *Inorg. Chem.*, 2020, **59**, 11377–11384.

57 E. A. Akam, R. D. Utterback, J. R. Marcero, H. A. Dailey and E. Tomat, Disulfide-masked iron prochelators: Effects on cell death, proliferation, and hemoglobin production, *J. Inorg. Biochem.*, 2018, **180**, 186–193.

58 C. Mertens, E. A. Akam, C. Rehwald, B. Brune, E. Tomat and M. Jung, Intracellular Iron Chelation Modulates the Macrophage Iron Phenotype with Consequences on Tumor Progression, *PLoS One*, 2016, **11**, e0166164.

59 E. A. Akam, T. M. Chang, A. V. Astashkin and E. Tomat, Intracellular reduction/activation of a disulfide switch in thiosemicarbazone iron chelators, *Metallomics*, 2014, **6**, 1905–1912.

60 Q. Wang and K. J. Franz, The hydrolytic susceptibility of prochelator BSIH in aqueous solutions, *Bioorg. Med. Chem. Lett.*, 2017, **27**, 4165–4170.

61 C. Srinivasan, A. Liba, J. A. Imlay, J. S. Valentine and E. B. Gralla, Yeast lacking superoxide dismutase(s) show elevated levels of "free iron" as measured by whole cell electron paramagnetic resonance, *J. Biol. Chem.*, 2000, **275**, 29187–29192.

62 G. P. Holmes-Hampton, N. D. Jhurry, S. P. McCormick and P. A. Lindahl, Iron content of Saccharomyces cerevisiae cells grown under iron-deficient and iron-overload conditions, *Biochemistry*, 2013, **52**, 105–114.

63 A. L. Cockrell, G. P. Holmes-Hampton, S. P. McCormick, M. Chakrabarti and P. A. Lindahl, Mössbauer and EPR Study of Iron in Vacuoles from Fermenting Saccharomyces cerevisiae, *Biochemistry*, 2011, **50**, 10275–10283.